APPENDIX H: METHOD FOR ESTIMATING TIME-DEPENDENT FAULT HAZARD IN THE ABSENCE OF AN EARTHQUAKE RECURRENCE RECORD

TABLE OF CONTENTS

LISTS OF TABLES AND FIGURES

Tables

Figures

ABSTRACT

Under the principles of probabilistic seismic hazard analysis (PSHA), technically defensible models of fault behavior must be included in the analysis. The model most commonly used in PSHA for earthquake occurrence, the Poisson model, cannot directly accommodate time dependence. Nevertheless, time-dependent earthquake recurrence has been reported at paleoseismic sites in California and elsewhere, and a general model of time dependence can be anticipated under a mechanical model of secular tectonic fault loading with quasi-periodic failure in earthquakes. For faults with a long paleoseismic record and a documented most recent event, time dependence can be incorporated into PSHA using other recurrence models. We present here a new method for incorporating time dependence when little more than the fault slip rate is known about the fault of interest. We call the estimate the Equivalent Poisson Ratio (EPR), since it is not an absolute estimate of time-dependent hazard, but rather a ratio applied to a time-independent hazard estimate developed by conventional PSHA methodologies.

Fault slip rate can be used with bounds on potential displacement per event to develop a range of possible earthquake recurrence intervals. Each recurrence interval is associated with a conditional survival function that describes the probability of an open interval of any given length since the last fault-resetting event. A crafted likelihood approach based on the joint probability of the recurrence interval and time since the most recent event leads to an EPR estimate for any given coefficient of variation (CV) of the time-dependent model functional form. Weighting by likelihood across values of CV leads to the final EPR estimates. We express them in terms of a three-point cumulative distribution approximation, and use the branch-weighted-mean EPR where a single EPR value is desired. EPR estimates depend on the ratio of the open time since the most recent event (tMRE) to the recurrence interval, and tend to 1.0 as the ratio approaches 0.

We illustrate the method with nominal values from two faults near the coast of Central California that contribute to the site-specific seismic source characterization at the Diablo Canyon Power Plant (DCPP). The branch-weighted-mean EPR estimate for the Hosgri fault using the lognormal recurrence distribution and a minimum $tMRE$ = 242 years is 1.24 (1.09–1.33) for a fault slip rate of 1.7 (0.7–2.7) mm/yr, where the range reflects the 8.5% and 91.5% values of a continuous distribution. Using the same tMRE and recurrence model, a nominal slip rate of 0.26 (0.18–0.36) mm/yr for the Los Osos fault yields an EPR estimate of 1.03 (1.02–1.04), which, considering the uncertainties involved, could be rounded to 1.0. Although the branch-weighted mean is essentially 1.0, three-point approximation points, 0.26, 1.16, and 1.54, can be carried forward, if desired into a logic tree with their corresponding weights of 0.25, 0.50, and 0.25. The upper limit physically corresponds to the weight of evidence that the fault is due or past due relative to its average.

We also show how even limiting evidence about the MRE from paleoseismic investigation can significantly increase the mean EPR. Although this methodology was developed in the course of the seismic source characterization (SSC) for the DCPP, the

results presented here should be considered only representative. Final values and implementation details are provided in the main SSC documentation.

H.1.0 INTRODUCTION

If ground-rupturing earthquakes occur randomly in time, their occurrence can be modeled as a Poisson process. If earthquakes instead release energy stored during a period of tectonic loading, they will be more likely to occur when the energy storage is high and less likely when it is low, including in the early time following an earthquake.

The model of elastic loading of faults by secular processes and sudden release in earthquakes was first articulated by Reid (1911). This model has given rise to end-member models for predicting earthquake timing and size. The time-predictable model (Shimazaki and Nakata, 1980) predicts failure time based on the slip in the previous event and a model of fixed fault strength. The alternative slip-predictable model makes no claim about when an earthquake will occur, but predicts the slip amount (~earthquake size) as a function of time since the previous event. Neither model has proven entirely satisfactory (e.g., Weldon et al., 2004), but in environments where secular loading occurs, release in occasional, perhaps temporally irregular, earthquakes is now generally accepted.

The concept of time-dependent earthquake occurrence in probabilistic seismic hazard analysis (PSHA) applies to fault-specific seismic sources. The inter-event times for earthquakes distributed randomly in time as described by a Poisson model follow an exponential distribution. The exponential model for earthquake recurrence is attractive because it requires only one parameter, the mean inter-event time. Modeling earthquakes as being random in time is also attractive when little is known about inter-event times because the use of more complicated models with two or more parameters cannot be rigorously defended by their improved fit to data (Akaike, 1974). Another reason for the use of the Poisson (random in time) model is that regulatory design criteria are expressed as target annual frequencies of exceedance (e.g., 10^{-4}) without consideration of any time dependence. Given the prominence of the Poisson model of earthquake occurrence in PSHA, most computer codes for hazard estimation have, until recently, assumed the Poisson model. Recognition that earthquake occurrence may be time dependent creates interest in ways that current PSHA computer codes can be used and still model time-dependent sources. Equivalent Poisson Ratio estimates are the relative adjustments to time-independent rupture rates necessary to produce the equivalent time-dependent rupture rate.

Relying solely on the Poisson model of earthquake occurrence runs counter to another principle of PSHA: namely, that the price for lack of information is increased uncertainty. In this case, the lack of information about earthquake recurrence does not automatically justify use of the simplest available recurrence model. If an earth model of secular tectonic loading is considered credible, then a time-dependent recurrence model must also be part of the uncertainty in the hazard assessment.

We show in this paper that well-posed estimates of relative time-dependent seismic hazard can be developed from an estimate of fault slip rate and limited information about the time since the most recent event. We call the relative hazard estimate the Equivalent Poisson Ratio (EPR) because it is expressed as a ratio of the time-dependent to the time-independent hazard estimate. The EPR formulation can be applied in hazard codes as a constant that multiplies the time-independent hazard. Unknown parameters that affect the hazard estimate such as earthquake displacement per event (DPE) and the coefficient of variation (CV) of recurrence are included as geologically bounded ranges. The resulting estimates can be tested for robustness to alternative input parameters. We find that time-dependent EPR estimates are stable in the presence of reasonable alternative values for the contributing constraints. The method for estimating EPRs is developed in somewhat general terms, but where illustrations help the discussion, examples are drawn from a site-specific application on the central coast of California, the seismic hazard estimation at the Diablo Canyon Power Plant.

H.2.0 RECURRENCE MODELS

We will use $f(t; \boldsymbol{\theta})$ to refer to the probability density function (PDF) with distribution parameters $\boldsymbol{\theta}$ for intervals between ground-rupturing earthquakes, and $F(t; \boldsymbol{\theta})$ for the corresponding cumulative distribution function (CDF). Reference to $\boldsymbol{\theta}$ may be dropped when the role of the parameters is clear from the context. The conditional probability *CP* of an earthquake for a forecast period T_f starting at time t is then

$$CP\left(t;\, T_f, \boldsymbol{\theta}\right) = \frac{F\left(T_f + t\right) - F(t)}{1 - F(t)} \tag{H-1}$$

On Figure H-1, $CP(t;\, T_f, \boldsymbol{\theta})$ is the ratio of the area under the PDF from t to $t + T_f$ (dark gray) divided by the total area to the right of t (sum of the shaded areas). Two examples are shown on Figure H-1: the upper for an exponential distribution, and the lower for a lognormal distribution. The long-term mean (LTM) is the same for both distributions. The predictions of the two models differ most strongly at times that are short compared to the LTM.

If earthquakes are distributed randomly in time, the intervals between events have an exponential distribution (Figure H-1a) with a single parameter $\boldsymbol{\theta} = \lambda$, where λ is the LTM rate of earthquake recurrence:

$$f(t; \lambda) = \lambda e^{-\lambda t} \tag{H-2}$$

with cumulative distribution

$$F(t;\, \lambda) = 1 - e^{-\lambda t} \tag{H-3}$$

On Figure H-1, $\lambda = 1.0$. From Equation H-1 the conditional probability of an event in the next T_f years is then

$$\left[e^{-\lambda t} - e^{-\lambda\left(t + T_f\right)}\right] \Big/ e^{-\lambda t} = 1 - \, e^{-\lambda T_f} \, \approx \, \lambda T_f \tag{H-4}$$

where the final approximation applies when T_f is small compared to the recurrence interval. Thus, if the occurrence of earthquakes is described by a Poisson process, then the conditional probability of an event in some future time is independent of time and normally approximately equal to the annual rate times the forecast length T_f,.

For time-dependent recurrence models, the conditional probability depends on the time since the fault was reset. As an example, the lognormal probability distribution (Figure H-1b) characterizes variables whose logarithms are normally distributed with parameters $\theta = \{\mu, \sigma\}$ where μ is the mean log of interval lengths and σ^2 is the variance:

$$f_{LN}(t;\mu,\sigma) = \frac{1}{t\sigma\sqrt{2\pi}} e^{\frac{-(\ln(t)-\mu)^2}{2\sigma^2}} \quad \text{(H-5)}$$

The CDF of the lognormal distribution is

$$F_{LN}(t;\mu,\sigma) = \frac{1}{2} + \frac{1}{2}\,\mathrm{erf}\left(\frac{\ln(t)-\mu}{\sqrt{2}\,\sigma}\right), \quad \text{(H-6)}$$

where *erf(.)* is the error function. Substituting $F_{LN}(t; \mu,\sigma)$ into Equation (H-1) would confirm that the T_f-period conditional probability is time dependent.

The hazard function for continuous distribution functions expresses the instantaneous rate of an event as a function of time:

$$H(t;\theta) = \frac{f(t;\theta)}{1-F(t;\theta)} \quad \text{(H-7)}$$

Comparing the hazard functions for the exponential and lognormal distributions brings out a fundamental difference between the two. For any value of *t*, including as *t* approaches *0*, *H(t)* for the exponential distribution (Equation H-3) equals λ. Applied to earthquake recurrence, this means that the hazard from a ground-rupturing earthquake is the same immediately after one occurs as it was at any time before it. In contrast, $f_{LN}(t)$ and $F_{LN}(t)$ approach *0* as $t \rightarrow 0$, and $H_{LN}(t) = 0$. Thus, under the lognormal model, the hazard is small immediately after a large event.

Lognormal parameters μ and σ are related to the LTM recurrence rate λ by

$$1/\lambda = \exp(\mu + \sigma^2/2) \quad \text{(H-8)}$$

The arithmetic CV for the lognormal distribution is independent of μ and given by

$$CV = \sqrt{e^{\sigma^2} - 1} \quad \text{(H-9)}$$

If we know λ and σ, we can form a ratio of conditional probabilities between time-dependent and exponential models that share a common long-term mean (Figure H-2). As anticipated in our examination of *H(t)*, the conditional probability ratio (CPR) is zero just after the previous earthquake, increases to 1.0 when the time-dependent and time-independent forecasts are equal, and reaches a maximum that depends on the lognormal width parameter before declining.

After introducing two other time-dependent distributions for earthquake recurrence, we will focus on how to estimate hazard ratios when information about recurrence parameters and the time since the most recent event is limited.

The Brownian Passage Time (BPT) model of earthquake recurrence (Ellsworth et al., 1999; Matthews et al., 2002; WGCEP, 2003) is an application of the inverse Gaussian distribution. It models recurrence in terms of a secular loading rate, around which are random Gaussian deviations representing local strain increases or decreases. The BPT PDF can be formulated in terms of two variables, η and α:

$$f(t;\, \eta, a) = \left(\frac{\eta}{2\pi a^2 t^3}\right)^{\frac{1}{2}} exp\left(\frac{(t-\eta)^2}{2a^2\eta t}\right) \qquad \text{(H-10)}$$

Location parameter η characterizes the secular loading rate. Numerically, η is the arithmetic mean of the interval lengths and equal to the reciprocal of λ from the exponential distribution. Parameter α is numerically the CV, although Matthews et al. (2002) prefer the term *aperiodicity* on mathematical grounds. The BPT model can have a wider variety of shapes than the lognormal distribution, but the two are similar for parameters likely to come from paleoseismic data.

We also consider the Weibull distribution. The Weibull distribution is sometimes applied to forecast probabilities of a large earthquake because of its more common use in modeling time-to-failure rates in mechanical or engineered systems. The PDF for Weibull random variables and $t \geq 0$ is

$$f(t;\, \nu, k) = \frac{k}{\nu}\left(\frac{t}{\nu}\right)^{k-1} \exp\left(-\left(\frac{t}{\nu}\right)^{k}\right) \qquad \text{(H-11)}$$

Parameter ν governs the width of the distribution. Comparison of the Weibull cumulative distribution

$$F(t;\, \nu, k) = 1 - \exp(-\left(\frac{t}{\nu}\right)^{k}) \qquad \text{(H-12)}$$

to Equation (H-3) shows that parameter k controls the shape of the Weibull distribution relative to an exponential. For $k = 1$ the Weibull distribution reduces to the exponential distribution. For $k > 0$, the failure rate increases monotonically with time.

H.3.0 INCLUDING UNCERTAINTY IN CONDITIONAL PROBABILITY RATIOS

Our strategy to generalize CPRs begins with knowledge of the slip rate on the fault for which we seek the hazard. Values for slip rate typically are developed through geologic investigations. Initially, we consider slip rate r, in mm/yr, without uncertainties, but will return to include uncertainties after the basic method is set out.

We parlay the fault slip rate into a set of mean recurrence rates by dividing the slip rate into a set of candidate mean slips per event D. For estimating time dependence, it is the future slip that matters. Since this is unknown, we instead propose a distribution of D

consistent with the state of knowledge from the fault of interest, or from similar faults. Two such example distributions are shown on Figure H-3.

The two curves on Figure H-3 model DPE on two types of fault. The broader distribution (solid line) is designed to apply to moderate strike-slip faults such as the Hosgri fault off the coast of Central California. The distribution conveys a relative agnosticism among choices in DPE from 1.5 meter (m) to 3.0 meters per event (m/event), with tolerance for values as small as 0.5 m and non-zero probabilities up to 5.5 m/event. How, one might ask, can bounds on DPE be offered? One approach is to look at previous ground ruptures in the region. In California, for example, the largest measured average slips per event on the San Andreas fault are 4.45 m/event and 4.3 m/event for the 1857 and 1906 earthquakes, respectively (Biasi et al., 2013). Limited available slip-per-event data from previous such events (Zielke et al., 2010) suggest similar, but not likely larger, events in the past. Using an upper bound of 5.5 m/event reflects the possibility that not all is known about California's strike-slip faults. The second curve on Figure H-3 (dashed) was constructed for application to smaller faults. It expresses some geological confidence, perhaps from paleoseismic investigations or fault-length scaling, that slips of 1.0–2.5 m average per event are most likely, but that a range of 0.5–4.0 m/event are at least minimally credible for the fault. The actual distributions are parametric inputs, so it is straightforward to evaluate whether any choices are strongly influential. In practice, EPR results are not strongly sensitive to reasonable choices for the shape of the DPE set.

We calculate LTM earthquake recurrence times by dividing DPE by the fault slip rate. The probabilities of each possible LTM value are copied from the DPE distribution. For each LTM value, $1/LTM = \lambda$ can be used in the time independent Poisson distribution and the LTM itself is the basis for the location parameter of time-dependent distributions.

The width parameter of the time-dependent PDF governs how regularly or irregularly earthquakes occur on the fault. As with the LTM, a precise estimate is not available, but an informed range can be offered. Figure H-4 shows two distributions that express somewhat different views of the CV distribution. The solid line is patterned after the range observed at high-quality paleoseismic sites on California strike-slip faults. It expresses greatest confidence in CV values between 0.5 and 0.8, and less confidence in very regular ($CV < 0.5$) or more random recurrence. This range bounds 10 of 11 well characterized California paleoseismic records (Biasi, 2013; Weldon et al., 2013). By emphasizing this range, we express some confidence that the Hosgri fault in California would fall in a similar range, but recognize also that more or less regular recurrence is possible. The second distribution on Figure H-4 (dashed) represents a less clear range designed for dip slip faults. Mechanically, dip slip faults do not have as strong a continuity of motion requirement as strike-slip faults. Unfortunately at present dip slip faults are not as well characterized as strike slip faults. Consequently a wider range of CV values is considered credible; the effect is to add uncertainty in the CV range. As with the DPE distributions, we will find that EPR estimates do not strongly depend on the CV distribution.

The conditional probability of a future event in a time-dependent model depends on the time since the most recent event (tMRE). The most recent event for hazard purposes is defined as the event that resets the clock for occurrence of ground rupturing earthquakes. One of two types of tMRE constraints are available for most faults. The first is an inequality constraint, $tMRE > T_{min}$, that sets some minimum time in the past after which no resetting event is believed to have occurred. In most places a minimum tMRE of some decades can be given based on instrumental records (Felzer, 2013). In much of southern California, records from Spanish missions allow an estimate of $tMRE > 200$ years (Toppozada et al., 1981). A pre-historic minimum tMRE might be developed from a paleoseismic record where the most recent ground rupture is dated but the magnitude of the event, and thus the time of fault resetting is uncertain. The second type of tMRE constraint is an equality relation, $tMRE = T_{eqk}$. Historical events in California in this category include the 1857 Fort Tejon and 1906 San Francisco earthquakes. An equality constraint could also apply if paleoseismic data were of such good resolution and strike extent that a single large event is the only credible explanation. Such an event near 1720 A.D. seems required to explain paleoseismic evidence on the southern San Andreas fault (Sieh 1986; Seitz and Williams, 2007; Philibosian et al., 2011; Haaker et al., 2013).

H.4.0 ESTIMATING EQUIVALENT POISSON RATIOS

With the necessary components in hand, we now consider the process of estimating EPRs. We use a lognormal distribution in the explanation (Figure H-5), planning to include the BPT and Weibull distributions afterward. In outline, the process is in two parts. The first part is to generalize conditional probability calculations to cover the full range of possible recurrence intervals and possible times since the most recent event for each considered CV value. We use the term “conditional probability ratio” to refer to ratios made without reference to the weight or probability given to the input values. The EPR is extracted from the CPR by weighting inputs such as the DPE and minimum time since the most recent event. In the realm of seismic source characterization, the EPR thus includes judgments and weights on input values, while the CPR covers a range of input values without reference to their credibility. The range of possible CV values is included by treating the CV as an epistemic unknown (Figure H-4). EPR estimates for a given CV are combined in the end according to CV weights. Fault slip rate is constant within individual EPR estimates, and slip rate uncertainty is included by combining EPR estimates using slip rate weights as an epistemic uncertainty.

Figure H-5 summarizes the calculations leading to conditional probability ratios for three assumed values of LTM, a $CV = 0.6$, and a fault slip rate of 1.7 mm/yr, the current best estimate for the Hosgri fault. LTM values of 500, 1000, and 2,000 years were used on Figure H-5. These LTM values correspond to 0.85, 1.7, and 3.4 meter (m) average DPE values, respectively – similar to the expected range on many faults in California. Lognormal PDFs for the three LTM values are shown on Figure H-5a. In Figure H-5b we show the survivor functions $S(t) = 1-F(t)$. $S(t)$ is also known as the complementary cumulative distribution. The survivor function for a given LTM describes how probable any given wait time would be since the MRE. For example, for an LTM of 1,000 years,

the median recurrence interval would be approximately 800 years, and the wait time should be ≤2,550 years 97.5% of the time (circle symbol). The 97.5% limit is proportional to LTM; for $CV = 0.6$, tMRE will be less than $2.55 \times LTM$. The ratio increases with CV, corresponding to increasing weight in the right tail of the PDF. For each LTM, conditional probabilities of ground rupturing earthquakes can be calculated across the range of times since the MRE (Figure H-5c). Numerically, 30-year forecasts have been used. For the renewal-based earthquake recurrence models, there is a range of tMRE and LTM in which time-dependent conditional probabilities are smaller than corresponding time-independent estimates. However, for most of the likely range of tMRE, the CPR is larger than 1.0, indicating that the time-dependent hazard is greater than the corresponding Poisson rate. This range in hazard is the origin of the EPR. The ratio (Figure H-5d) peaks near the mode of the lognormal PDF, then declines with increasing tMRE. Plots on Figure H-5d end at the upper 97.5% point of their respective survivor functions (circles, Figure H-5b) to make the point that greater values of tMRE would be increasingly inconsistent the respective assumed values of LTM and CV. In addition to being internally consistent, this approach of focusing attention on the probable range of tMRE minimizes the impact of differences in asymptotic behavior between the lognormal, Brownian Passage Time, and Weibull recurrence distribution models.

The effect of constraints on $tMRE > T_{min}$ can be anticipated on Figures H-5c and H-5d. Suppose, for example, that $tMRE < 500$ years could be eliminated by a paleoseismic constraint. Then even without definite information on the true value of tMRE or the LTM, any weighted combination of the remaining portions of the CPRs on Figure H-5d would lead to an EPR in the range of 1.6–1.7 for this CV.

The conditional probability ratio lines on Figure H-5d can be generalized into a surface using the complete range of tMRE and LTM (Figure H-6). A grid is constructed by dividing ranges of LTM and tMRE into small increments ΔLTM and $\Delta tMRE$, respectively. An increment of 20 years was used for both. Each of the lines on Figure H-5d becomes a row on Figure H-6, except for not being truncated at its 97.5% limit. The peak of the conditional probability ratio surface trends linearly with LTM on Figure H-6 because for a given CV, the shapes of the underlying recurrence PDFs (Figure H-5a) are self-similar. The CPR surface on Figure H-6 is a mathematical construct that does not consider the likelihood of any particular values of LTM and tMRE.

We now require a means to associate weights with the gridded CPR values on Figure H-6. Conceptually this can b done by dividing the CPR into small discrete ranges, then for each, summing the weight associated with that range. We form a joint probability surface W on the same LTM-tMRE grid. The LTM probability distribution comes from the input displacement-per-event distribution and a slip rate of 1.7 mm/yr. The probabilities for individual discrete values LTM_i are found by finely resampling the LTM PDF, then renormalizing to give a unit total probability. For each value LTM_i there is a row with the corresponding survivor function $S(tMRE) = 1-F(t)$. The probability for the unknown time since the last event, given the recurrence rate and CV, is given by the survivor function. The discretized $S(tMRE)$ is normalized to sum to unit area so it can be applied to the grid. Numerically, values on the joint probability grid are given by:

$$W_{ij} = p(LTM_i)S\left(tMRE_j|LTM_i\right) \quad \text{(H-13)}$$

Each row in the weighting grid is a complete PDF conditioned on $LTM = LTM_i$. Summing W_{ij} over j yields LTM_i, and the sum over $LTM_i = 1$ by construction. The resulting joint probability surface for CV=0.6 is concentrated above the diagonal *LTM = tMRE* because of the shape of *S(t)*. Probabilities decline with largest allowed values of LTM because they are associated with declining probabilities of the largest allowed displacements per event (Figure H-2). In Figure H-7 the joint probability surface has been normalized by its maximum value so that the contours numerically reflect relative weight on a scale from 0 to 1.

Weighting of the CPR surface (Figure H-6) is applied in two steps. First, the CPR is sorted from largest to smallest in an equivalent one-dimensional array, *CPR(K)*, where *K* is the sort order, and *k* indexes *K*. The same "sort" order *K* is applied to *W*. The cumulative sum of *W(K)* is denoted as *F(W)*. *F(W(k))* gives the weight (probability) that the weighted CPR is equal or greater than *CPR(k)*. Pairs of *CPR(k) vs. F(k)* are plotted on Figure H-8. Because weights are now applied to the CPR, we call Figure H-8 the equivalent Poisson ratio for this CV. In subsequent plots we will summarize EPR values in terms of a three-point distribution (Miller and Rice, 1983) suitable for use in a logic tree. Stars on Figure H-8 mark the 91.5%, 50%, and 8.5% distribution values. EPR values for these points are multiplied by [0.25, 0.50, 0.25], respectively, to obtain the weighted mean EPR value for this CV.

In explaining the joint LTM-tMRE surface, we used $tMRE > T_{min} = 0$. In effect this means that a ground-rupturing earthquake could have occurred last year. Focusing for the moment on the central California coast, older T_{min} values might be considered. The inauguration of the Southern California Seismic Network in 1932 would lead to $T_{min} > 82$ years. The founding of San Luis Obispo as a city, and establishment of a newspaper, and road and rail connections in the 1870s would give a fairly secure $T_{min} = 144$ years. Felzer (2013) estimates the magnitude of completeness for the central California coastal region since this time to be $M \geq 6.5$. Finally, the Spanish mission record at San Luis Obispo starts in 1772 and appears to be fairly complete. This would allow some confidence for large events in $T_{min} = 242$ years. We implement the constraint $tMRE > T_{min}$ by removing the range $t < T_{min}$ in *S(t)* and renormalizing. Mathematically, *S(t)* is replaced by $S(t|t>T_{min})$. EPR values for these four cases and a distribution CV of 0.6 are shown on Figure H-9. Dashed lines on Figure H-9 are weighted mean EPRs, matched to the curves by color and symbol type. This figure shows that even weak historical limits on tMRE directly influence the CPR estimate. tMRE constraints remove the early time portion of the CPR where the ratio is less than 1.0 and the time-dependent hazard is smaller than the time-independent. The remaining range is thus concentrated in CPR ratios greater than 1, which raises the net weighted EPR value. The effect of T_{min} diminishes as it becomes a smaller fraction of the mean recurrence time.

If the date of the relevant MRE is known, the equality constraint $tMRE = T_{eqk}$ can be applied. With the equality constraint, there is no weighting to be done across the range of

tMRE, and *W* for calculating the EPR reduces to the weights in a single column at *tMRE* = T_{eqk}.

We plot weighted mean EPR values for all considered values of CV and three fault slip rates on Figure H-10. In general EPR estimates will vary with CV. In this case EPR values are larger for small CV values because their recurrence PDFs are narrower and concentrate more weight in the forecast period (e.g., Figure H-5d).

To arrive at final estimates of EPR for the assumed slip rate, we weight the three-point values of EPR estimates (e.g., Figure H-8) by the CV weighting shown on Figure H-4. Figure H-11 provides final values for the three fault slip rates, with their corresponding three-point values. As shown on Figure H-11, EPR estimates are stable, varying in a predictable relationship to fault slip rate. Upper branch (91.5%) values are consistently around 1.85, corresponding to an interpretation that rupture is "due". Physically, the fault has accumulated at least 1.7 mm/yr*242 yr = 0.41 m of slip since the latest allowed MRE. High estimates of EPR gather weight from smaller allowed values of CV and from the smaller range of allowed DPE for which rupture would be more imminent. The available data allow these combinations, so from a PSHA standpoint they must be part of the range of the EPR estimate. At the same time, to increase the EPR much further would require affirmative data for a lower range of CV. On the small end, with 8.5% weight, the EPR could be as low as 0.16 to 0.58. These values draw most of their weight from combinations of large DPE and large CV. Large DPEs correspond to long recurrence intervals and a smaller ratio of T_{min} to the recurrence interval. Branch-weighted-mean EPR values using the method of Miller and Rice (1983) are calculated using $0.25*EPR_{8.5\%} + 0.50*EPR_{50\%} + 0.25*EPR_{91.5\%}$. We obtain branch-weighted-mean EPR estimates for the Hosgri fault of 1.09, 1.24, and 1.33 for slip rates of 0.7, 1.7, and 2.7 mm/yr, respectively (Table H-1).

Table H-1. Moderate Slip Rate Fault Three-Point Distribution and Branch-Weighted Mean (BWM) EPR for Three Recurrence Distributions and Several Values of tMRE

Fault	PDF	Slip Rate	tMRE	8.5%	50%	91.5%	BWM
Hosgri	LN	1.7	242	0.39	1.35	1.85	1.24
Hosgri	LN	0.7	242	0.15	1.18	1.86	1.09
Hosgri	LN	2.7	242	0.58	1.46	1.84	1.33
Hosgri	LN	1.7	0	0.04	1.05	1.83	0.99
Hosgri	LN	1.7	82	0.15	1.16	1.84	1.08
Hosgri	LN	1.7	144	0.24	1.24	1.84	1.14
Hosgri	LN	0.7	144	0.10	1.12	1.86	1.05
Hosgri	LN	2.7	144	0.38	1.32	1.82	1.21
Hosgri	BPT	1.7	242	0.42	1.35	1.81	1.23
Hosgri	WBL	1.7	242	0.59	1.08	1.92	1.17

EPR estimates for low slip-rate faults follow the above outline. Table H-2 gives EPR results for a nominal slip-rate estimate set of the Los Osos fault, which is thought to slip at a rate an order of magnitude slower than the Hosgri fault. Estimates are given for two values of minimum tMRE. The main difference for low slip-rate faults is that it takes more time to accumulate enough slip for a moderate or large earthquake. The ratio of tMRE to the recurrence interval determines the influence of the open interval. This ratio is small for low slip rate faults, causing the branch-weighted-mean EPR values to be only slightly greater than 1.0. In Table H-1, the extreme case of $tMRE = 0$ is thus an end-member, and within the resolution, 1.0.

We can use our EPR estimation tools to explore the value of paleoseismic data to the EPR estimate. To do this we adopt the nominal slip rate of 0.26 mm/yr, the same as for the Los Osos fault, but use a hypothetical minimum tMRE of 2,000 years. Under this scenario, the branch-weighted-mean EPR increases to 1.21 (Table H-2), or about a 20% increase in the mean time-dependent hazard compared to an EPR estimate with no meaningful constraint on the date of the MRE.

Table H-2. Low Slip Rate Fault Three-Point Distribution and Branch-Weighted Mean (BWM) EPR for Two Values of tMRE

Fault	PDF	Slip Rate	tMRE	8.5%	50%	91.5%	BWM
Los Osos	LN	0.26	242	0.26	1.16	1.54	1.03
Los Osos	LN	0.18	242	0.24	1.16	1.54	1.02
Los Osos	LN	0.36	242	0.29	1.17	1.53	1.04
Los Osos	LN	0.26	144	0.21	1.15	1.54	1.01
Los Osos	LN	0.18	144	0.20	1.15	1.54	1.01
Los Osos	LN	0.36	144	0.23	1.15	1.53	1.02
Hypothetical	LN	0.26	2000	0.67	1.32	1.54	1.21

H.5.0 PARAMETRIC EVALUATION

In this section we explore the robustness of EPR estimates to the choice of recurrence functional form and the difference between inequality and equality constraints on tMRE.

On Figure H-12 we compare survivor functions and EPR given CV for the lognormal, BPT, and Weibull distributions. We use a fault slip rate at 1.7 mm/yr, an LTM value of 700 years, and a range of CV values. Lognormal and BPT models are most similar to one another (Figure H-12). For both models and most CV values, the survivor functions near $S(t) = 1$ decrease slowly at first, corresponding to low probabilities of an event just after the MRE. In contrast the Weibull $S(t)$ function decreases immediately, especially for smaller CV values. When $tMRE < T_{min}$ is removed, so is the early low probability portion of the Weibull distributions. As a result, Weibull EPR values reach a factor of two or more larger values than either of the other two models. The monotonic increase in hazard with tMRE for the Weibull distribution can also be seen.

At first it might appear that the increase in conditional probability values with tMRE, especially for the Weibull distribution and small CV values (Figure H-12c), could destabilize the EPR estimate. However, weighting by the CV distribution (Figure H-13) reduces this tendency. Instead of diverging, the net branch-weighted-mean EPR estimates (dotted lines on Figure H-13) are similar to those for the other recurrence models.

On Figure H-14 values of CV-weighted EPR for a slip rate of 1.7 mm/yr and T_{min} =242 years are shown for the three time-dependent recurrence models considered. The lognormal points are repeated from Figure H-11. The BPT estimates are seen to be very close to the lognormal values. Results from the Weibull distribution differ from the other two, being about 20% lower at the mid-point, but slightly higher on both ends. If the Miller and Rice (1983) weights of [0.25, 0.50, 0.25] are applied to the 8.5%, 50%, and 91.5% points, weighted mean EPR estimates of 1.24, 1.23, and 1.17 are obtained for the lognormal, BPT, and Weibull models, respectively. These values can be interpreted as the mean time-dependent hazard increase. Most of the mean hazard increase comes from the information T_{min} = 242 years.

Finally, the large earthquake on the San Andreas fault in 1857 provides an opportunity to compare results of the constraint $tMRE > T_{\min}$ to $tMRE = T_{eqk}$ = 157 years. The 1857 M 7.8 event ruptured the fault from Parkfield southeast to beyond Wrightwood (Zielke et al., 2010). The magnitude and length of this rupture makes it a strong candidate as a resetting event, and since 1857 there have been no significant ground ruptures on the fault. The San Andreas fault slips at a rate of 30.3 mm/yr on the Cholame section at its nearest approach to DCPP, for a total of almost 4.8 m of slip since 1857. Figure H-15 compares three-point distributions for constraint $tMRE > T_{\min}$ and $tMRE = T_{eqk}$. The two estimates are similar, with branch-weighted mean values of 1.28 vs. 1.34, respectively. Since the fault is at or somewhat beyond the average recurrence interval, the equality constraint preferentially focuses near maxima of the conditional probability surface. The inequality constraint $tMRE > T_{\min}$ includes more of the declining CPR values at larger tMRE (e.g., the right side of Figure H-6). Since the equality constraint better represents the time dependence of the San Andreas fault, we use it to weight the fault's sources. For cases where the choice is less clear, some weighted combination of the two results may be preferred.

H.6.0 DISCUSSION

Our approach for estimating EPR depends on the estimate of fault slip rate. In practice, fault slip rates are uncertain. In principle, slip rate uncertainties might be propagated directly into uncertainties in LTM and tMRE probabilities. This would, however, introduce an additional, potentially severe, layer of complexity. The simpler approach that we have taken is to link EPR estimates directly to the epistemic range of slip rate values and weights from geologic studies. In the present case, the Hosgri fault slip rate is expressed in a three-point distribution with rates of 0.7, 1.7, and 2.7 mm/yr and weights 25%, 50%, 25%, respectively. These weights can be applied consistently to their respective EPR estimates because the slip rate and EPR estimates are causally linked.

Our approach to estimating EPRs uses units of real years. We chose this approach to keep the discussion more familiar to practicing geoscientists. Individually, components of the EPR estimation process might be normalized, such as expressing the LTM in terms of a range around some mean value (e.g., Figure H-2; see also Matthews et al., 2002; WGCEP, 2008). However, when the normalized LTM is used to weight probabilities of time since the most recent event, the joint probability surfaces (Figure H-7) become difficult to interpret directly, since T_{min} is a different fraction of LTM on every row. The forecast window would also have to be scaled.

Our estimates of EPR are conditioned on the shape of the recurrence distribution and rely on the linkage of LTM to plausible values of tMRE (e.g., Figure H-5b) through the survivor function. Combinations of LTM with tMRE greater than many multiples of LTM are strongly down-weighted for lognormal, BPT, and Weibull functional forms. One might ask, what if tMRE really is many multiples of the LTM? In such a case we would conclude that the data have impeached the condition on model functional form, and that an alternative recurrence model must be sought. Nothing in the method would prevent, for example, use of a strongly bi-modal event recurrence model.

Weighting the range of tMRE values by the corresponding survivor function $S(t|LTM)$ addresses a potential concern sometimes raised about the differences in asymptotic hazard between the lognormal and BPT models (e.g., Matthews et al., 2002). The lognormal model hazard function $f(t)/[1-F(t)]$ declines for $t >> LTM$, while the BPT model asymptotically approaches the Poisson rate. However, when we weight either distribution by its survivor function (Figure H-5b), the contribution of $tMRE >> LTM$ declines to unimportance. This property of the survivor function is an important part of why EPR estimates are relatively insensitive to the choice of recurrence model functional form.

We have not attempted to present EPR calculations for every permutation of knowledge that might be developed in a site-specific seismic source characterization. For example, we illustrate the consequences of different discrete values of T_{min}, with the intention that the choices be adopted in a logic tree format with individual weights. This corresponds better with the interpretation of T_{min} as an epistemic uncertainty, but the method could be extended to a continuum estimate of T_{min} if data became available to warrant the effort. Similarly, in principle, if one knew the magnitude-frequency distribution (MFD) on the fault of interest, that information could be used to shape the input DPE profile. In practice, MFDs for faults are rarely well known. In addition, the new appreciation of connectivity among faults (Field et al., 2013) has cast doubt on the classic understanding of fault MFDs. Displacement per event distributions might also be shaped by geologic observations. Hecker et al. (2013) report a relatively small range of displacements around a mean from repeated observations of displacements at a point. In their data, the observed range is typically on the order of ½ to 2× of mean displacement. However, this range is not dissimilar to the distributions we have used (e.g., Figure H-5). In any event we could not use their formulation without assuming a mean DPE, and any input DPE distribution peaked around a mean would effectively constrain the EPR by an unknown input.

Our approach to EPR involves a number of steps that might be criticized for want of rigorous inputs. Conspicuous opportunities include the *a priori* weights given to individual values of the DPE and CV distributions. Two replies can be offered. First, it is clear that some range of displacements per event and CV values must exist; the argument must be over how they are distributed. If a distribution is not known, but bounds can be suggested, then the least informative strategy is a uniform distribution on the bounds. Geologically, however, equal probabilities across the full range of world-wide DPE measurements from ruptures in continental crust (e.g., Wesnousky, 2008; Biasi et al., 2013) would be difficult to defend. At the same time there will be a middle range of DPE where being prescriptive about the relative weightings requires more information than is available. In this range, the DPE will be flat. This line of reasoning leads to DPE distributions like those we have used here. Our CV distributions follow the same logic. Figures 10 and 13 are provided in part so that the reader can assess the shifts in CV weight that would be needed to materially change the weighted EPR estimates. As with the DPE distribution, to depart from a bounded uniform distribution for CV requires particular knowledge that the CV of the Hosgri fault is very different from the well-studied strike-slip faults of California.

Our second reply is that a recurrence model that includes some sort of time dependence is intrinsically more complete than a model that ignores it.. It is entirely possible that the Hosgri fault is well past its average recurrence time. A time-independent PSHA would not naturally use this information. From a public safety standpoint, a purely time-independent model would leave out recurrence behavior that is frequently observed on active strike-slip faults. For the case of the Hosgri fault, defensible minimum times since the MRE of 144 and more likely, 242 years would raise the mean hazard estimate west of San Luis Obispo. Uncertainties in the functional form of the recurrence model, the slip rate, and elsewhere in the model preclude resolution to three decimal places, but our approach gives reasonable estimates to about two. Considering how little information is available as inputs, this seems somewhat remarkable.

Equivalent Poisson ratios assume faults are gradually being loaded and experience sudden release in fault rupture. This concept is expressed in the recurrence model functional forms that we have used in their estimation. At the western margin of central California, seismic and geodetic data give some confidence that processes at work and that the functional forms that describe recurrence elsewhere in the state can be applied here also. For sites where secular loading cannot be assumed, our EPR estimation method can be adapted if other functional forms of recurrence can be proposed. Ultimately, however, if nothing useful is known about the recurrence model, no magic in our approach to time dependent hazard can redeem the situation.

H.7.0 CONCLUSIONS

Modern seismic hazard analyses must include all technically defensible models for earthquake recurrence. Many paleoseismic investigations in California and elsewhere find some degree of time dependence in ground ruptures. Thus, absent strong evidence to the contrary, a time-dependent branch must be considered in evaluating hazard from fault

sources in California. In many cases, however, the need to estimate the potential hazard consequences from time dependence cannot be met with adequate data for the estimate. We present a new approach that yields a useful range of time-dependence estimates expressed as factors of the time-independent hazard rate. The method builds from a parameter likely to be available in a fault source study —the fault slip rate. The fault slip rate can be related to a range of possible earthquake recurrence rates through a bounded range of average DPE. A specially designed weighting method focuses probabilities and yields EPR estimates by CV. CV weighting informed by paleoseismic results in California lead to EPR values and distributions suitable for use in hazard estimation.

We find mean EPR estimates of 1.09, 1.24, and 1.33 for slip rates of 0.7, 1.7, and 2.7 mm/yr, respectively, applicable to the Hosgri fault in the near-offshore of central California, under the assumption that no significant Hosgri fault earthquake has occurred since the founding of the San Luis Obispo mission in 1772. Lower mean EPRs of 1.05, 1.14, and 1.21, respectively, result if the catalog of ground-rupturing earthquakes is considered complete only since the founding of San Luis Obispo around 1870. The influence of the open interval since the most recent event decreases as its fraction becomes smaller compared to the LTM recurrence interval. This trend is observed in our results for a low slip rate fault. With a rate of 0.26 mm/yr patterned on the Los Osos fault, the mean EPR is about 1.02. The mean EPR approaches 1.0 as *tMRE/LTM* approaches 0. We also show on the other hand that a paleoseismic constraint on a low slip rate fault can be useful for estimating the EPR, even when the MRE date can only be limited to being older than some age.

Time dependence as expressed in the EPR amounts to a direct relative increase in the estimate of seismic hazard compared to an analysis that omits it. The potentially prominent role of the EPR in seismic hazard estimates will attract attention, and undoubtedly future research into the topic. In the meantime, our approach offers a simple way to estimate time dependence to at least the first order, and thus provides a useful method for including time dependence in site specific PSHAs where tectonic loading is responsible for hazard-significant earthquakes.

H.8.0 REFERENCES

Akaike, H., 1974. A new look at the statistical model identification, *IEEE Transactions on Automatic Control* **19**: 716-723.

Biasi, G.P., 2013. Appendix H—Maximum Likelihood Recurrence Intervals for California Paleoseismic Sites: in Field, E.H., Biasi, G.P., Bird, P., Dawson, T.E., Felzer, K.R., Jackson, D.D., Johnson, K.M., and 11 others [Working Group on California Earthquake Probabilities], 2013. *Uniform California Earthquake Rupture Forecast, Version 3 (UCERF3)—The Time-Independent Model*, U.S. Geological Survey Open-File Report 2013–1165, 25 pp.

Biasi, G.P., Weldon, R.J., II, and Dawson, T.E., 2013. Appendix F—Distribution of Slip in Ruptures: in Field, E.H., Biasi, G.P., Bird, P., Dawson, T.E., Felzer, K.R., Jackson, D.D., Johnson, K.M., and 11 others [Working Group on California Earthquake Probabilities], 2013. *Uniform California Earthquake Rupture Forecast, Version 3 (UCERF3)—The Time-Independent Model*, U.S. Geological Survey Open-File Report 2013-1165, 41 pp.

Cornell, C.A., 1968. Engineering seismic risk analysis, *Bulletin of the Seismological Society of America* **58** (5): 1583-1606.

Cornell, C.A., and Winterstein, S.R., 1988. Temporal and magnitude dependence in earthquake recurrence models, *Bulletin of the Seismological Society of America* **78** (4): 1522-1537.

Ellsworth, W.L., Matthews, M.V., Nadeau, R.M., Nishenko, S.P., Reasenberg, P.A., and Simpson, R.W., 1999. *A Physically-Based Earthquake Recurrence Model for Estimation of Long-Term Probabilities*, U.S. Geological Survey Open-File Report 99-522, 22 pp.

Felzer, K.R., 2013. Appendix L—Estimate of the Seismicity Rate and Magnitude-Frequency Distribution of Earthquakes in California from 1850 to 2011: in Field, E.H., Biasi, G.P., Bird, P., Dawson, T.E., Felzer, K.R., Jackson, D.D., Johnson, K.M., and 11 others [Working Group on California Earthquake Probabilities], 2013. *Uniform California Earthquake Rupture Forecast, Version 3 (UCERF3)—The Time-Independent Model*, U.S. Geological Survey Open-File Report 2013-1165, 13 pp.

Field, E.H., Biasi, G.P., Bird, P., Dawson, T.E., Felzer, K.R., Jackson, D.D., Johnson, K.M., and 11 others [Working Group on California Earthquake Probabilities], 2013. *Uniform California Earthquake Rupture Forecast, Version 3 (UCERF3)—The Time-Independent Model*, U.S. Geological Survey Open-File Report 2013-1165/ California Geological Survey Special Report 228/ and Southern California Earthquake Center Publication 1792, 97 pp.

Field, E.H., Dawson, T.E., Felzer, K.R., and 8 others [2007 Working Group on California Earthquake Probabilities], 2008. *The Uniform California Earthquake Rupture Forecast, Version 2 (UCERF 2)*, USGS Open File Report 2007-1437, CGS Special Report 203, and SCEC Contribution 1138, 104 pp.

Haaker, E., Weldon, N., Weldon, R. and Rockwell, T., 2013. A high resolution Lake Cahuilla chronology to constrain earthquakes on the southern San Andreas system, *Southern California Earthquake Center Annual Meeting 2013 Proceedings Volume, XXIII, September 8-11, 2013*, abstract, p. 113.

Hecker, S., Abrahamson, N.A., and Wooddell, K.E., 2013. Variability of displacement at a point: Implications for earthquake-size distribution and rupture hazard on faults, *Bulletin of the Seismological Society of America* **103**: 651-674.

Matthews, M.V., Ellsworth, W.L. and Reasenberg, P.A., 2002. A Brownian model for recurrent earthquakes, *Bulletin of the Seismological Society of America* **92** (6): 2233-2250.

Miller, A.C., and Rice, T.R., 1983. Discrete approximation of probability distributions, *Management Science* **29**: 352-362.

Philibosian, B., Fumal, T., and Weldon, R., 2011. San Andreas fault earthquake chronology and Lake Cahuilla history at Coachella, California, *Bulletin of the Seismological Society of America* **101** (1): 13-38.

Reid, H.F., 1911. The elastic rebound theory of earthquakes, *University of California Publications: Bulletin of the Department of Geology* **6** (19), 413-444.

Seitz, G.G., and Williams, P., 2007. Development of a Long-Term Earthquake Record for Testing of Rupture Scenarios at the South End of the San Andreas Fault, Final Technical Report: U.S. Geological Survey External Grant, Awards Nos. 06HQGR0024 and 06HQGR0018, 17 pp.

Shimazaki, K., and Nakata, T., 1980. Time-predictable recurrence model for large earthquakes, *Geophysical Research Letters* **7** (4): 279-282.

Sieh, K.E., 1986. Slip rate across the San Andreas fault and prehistoric earthquakes at Indio, California, abstract T22C-01, *EOS Transactions, American Geophysical Union* (Fall Meeting Abstracts) **67** (44): 1200.

Toppozada, T.R., Real, C.R., and Parke, D.L., 1981. *Preparation of Isoseismal Maps and Summaries of Reported Effects for Pre-1900 California Earthquakes*, California Division of Mines and Geology Open-File Report 81-11, 182 pp.

Weldon, R., Scharer, K., Fumal, T., and Biasi, G., 2004. Wrightwood and the earthquake cycle: What the long recurrence record tells us about how faults work, *GSA Today* **14** (9): 4-10.

Weldon, R.J., II, Dawson, T.E., Biasi, G., Madden, C., and Streig, A.R., 2013. Appendix G—Paleoseismic Sites Recurrence Database: in Field, E.H., Biasi, G.P., Bird, P., Dawson, T.E., Felzer, K.R., Jackson, D.D., Johnson, K.M., and 11 others [Working Group on California Earthquake Probabilities], 2013. *Uniform California Earthquake Rupture Forecast, Version 3 (UCERF3)—The Time-Independent Model*, U.S. Geological Survey Open-File Report 2013–1165, 73 pp.

Wesnousky, S.G., 2008. Displacement and geometrical characteristics of earthquake surface ruptures: Issues and implications for seismic-hazard analysis and the process of earthquake rupture, *Bulletin of the Seismological Society of America* **98** (4): 1609-1632.

Working Group on California Earthquake Probabilities (WGCEP), 2003. *Earthquake Probabilities in the San Francisco Bay Region: 2002–2031*, U.S. Geological Survey Open-File Report 03-214, 253 pp.

Zielke, O., Arrowsmith, J.R., Ludwig, L.G., and Akçiz, S.O., 2010. Slip in the 1857 and earlier large earthquakes along the Carrizo Plain, San Andreas fault, *Science* **327** (5969): 1119-1122.

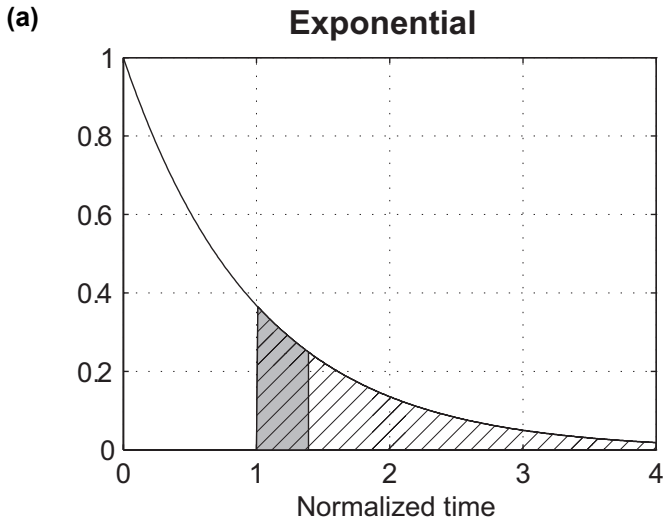

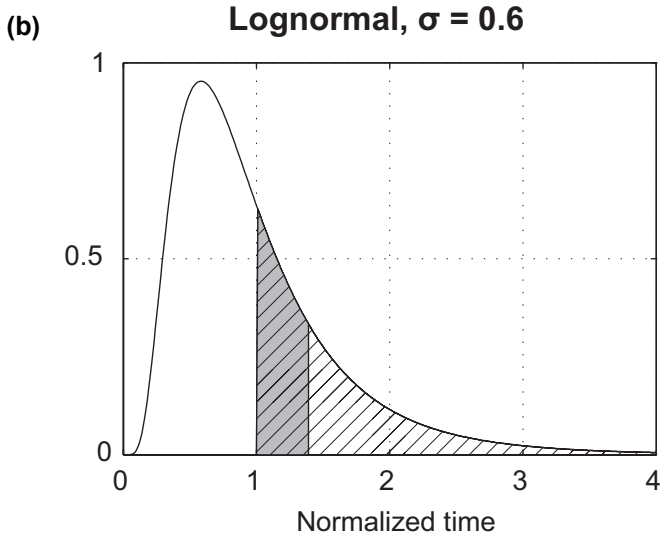

EXPLANATION

Area of forecast period

Total area

Note: The long-term mean is the same for both distributions shown.

Conditional Probability Calculation Illustrated for Exponential and Lognormal Earthquake Probability Distributions

DCPP SSC REPORT

Pacific Gas and Electric Company

Figure **H-1**

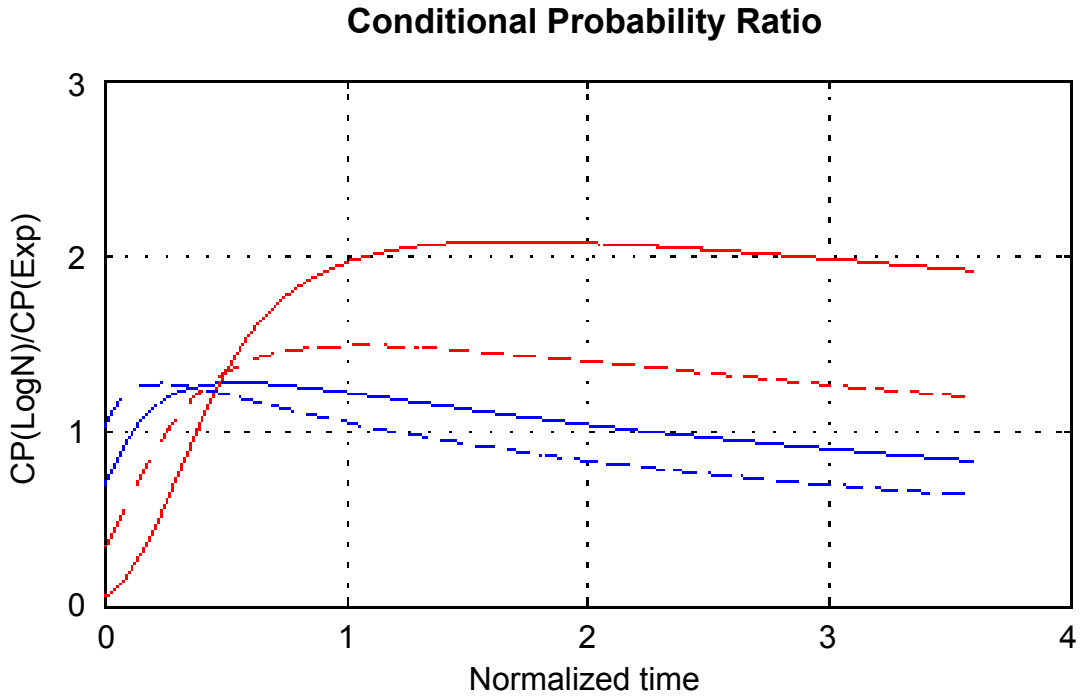

EXPLANATION

- σ = 0.4
- σ = 0.6
- σ = 0.8
- σ = 1

Conditional Probabilty Ratio for $\lambda = 1$, and $T_f = 0.4\lambda$

DCPP SSC REPORT

Pacific Gas and Electric Company

Figure **H-2**

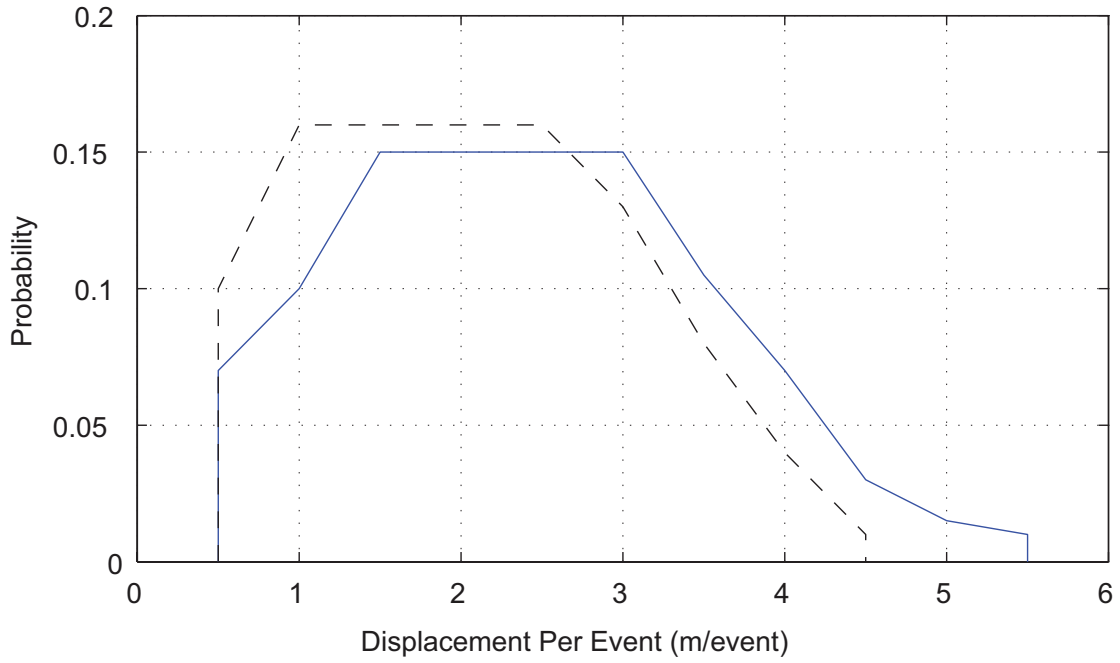

EXPLANATION

Hosgri

LOF, SLB

Displacement Per Event Models for the Hosgri and Los Osos or San Luis Bay Faults

DCPP SSC REPORT

Pacific Gas and Electric Company

Figure **H-3**

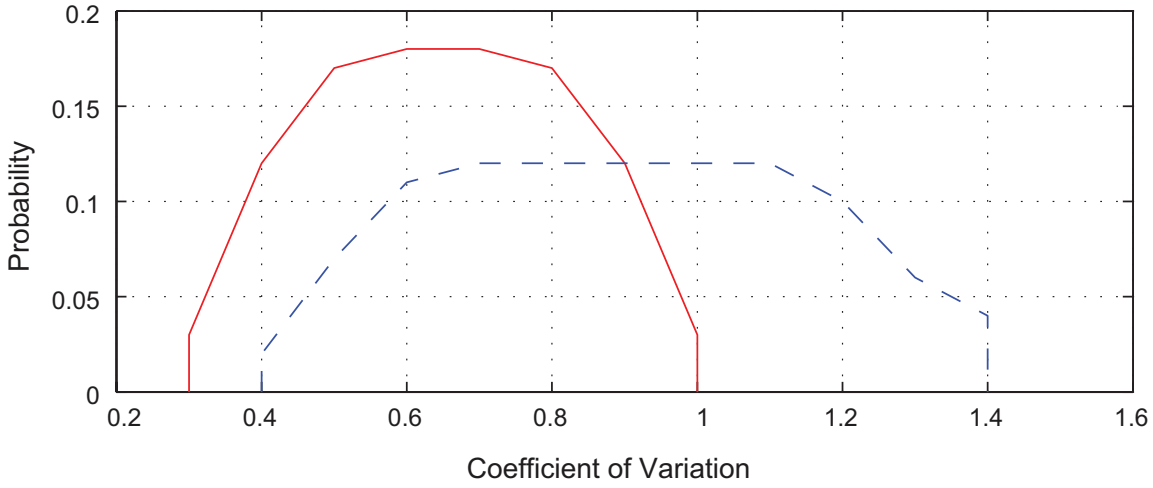

EXPLANATION

Strike Slip

Dip Slip

Two Probability Distributions of Coefficient of Variation Values

DCPP SSC REPORT

Pacific Gas and Electric Company

Figure **H-4**

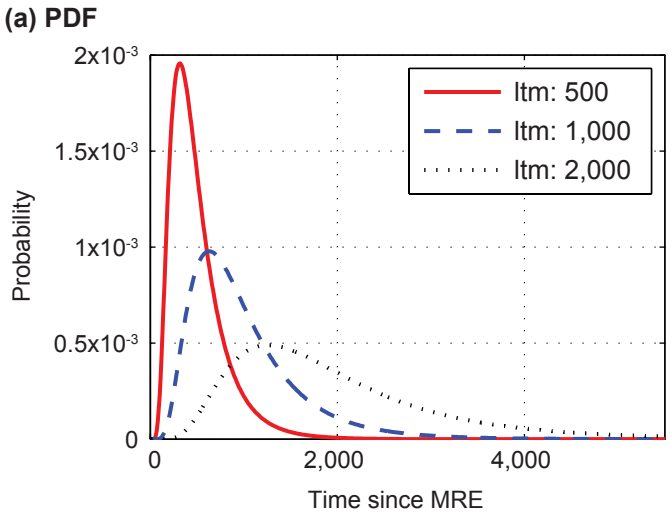

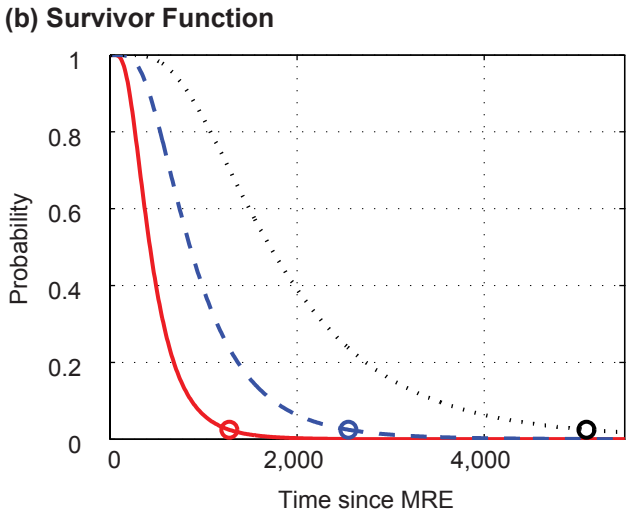

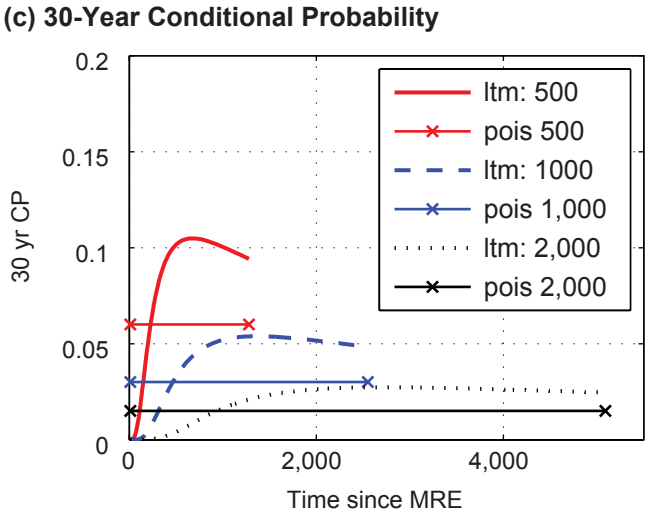

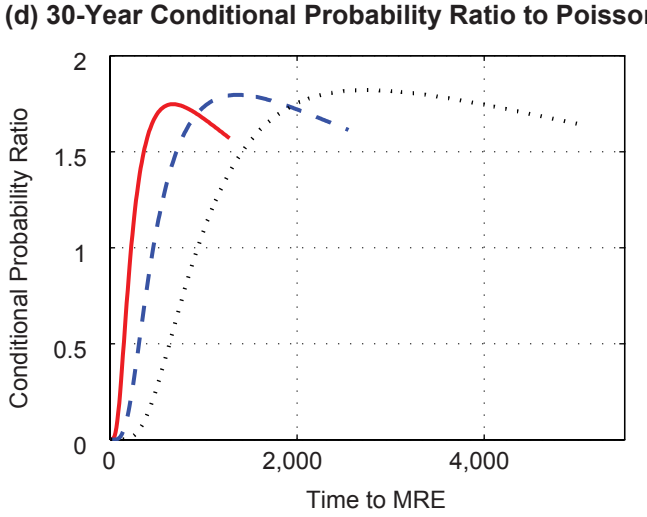

Notes:
- 97.5% of probability is to the left of circles on survivor functions (Panel (b)). The 30-year conditional probability (Panel (c)) and 30-year conditional probability ratio (Panel (d)) end at respective same points.
- For all plots shown, coefficient of variation is 0.6 and fault slip rate is 1.7 mm/yr.

Lognormal PDF, Survivor Function, 30 Year Conditional Probability, and 30 Year Conditional Probability Ratio for Three Values of Long-Term Mean

DCPP SSC REPORT

Pacific Gas and Electric Company

Figure **H-5**

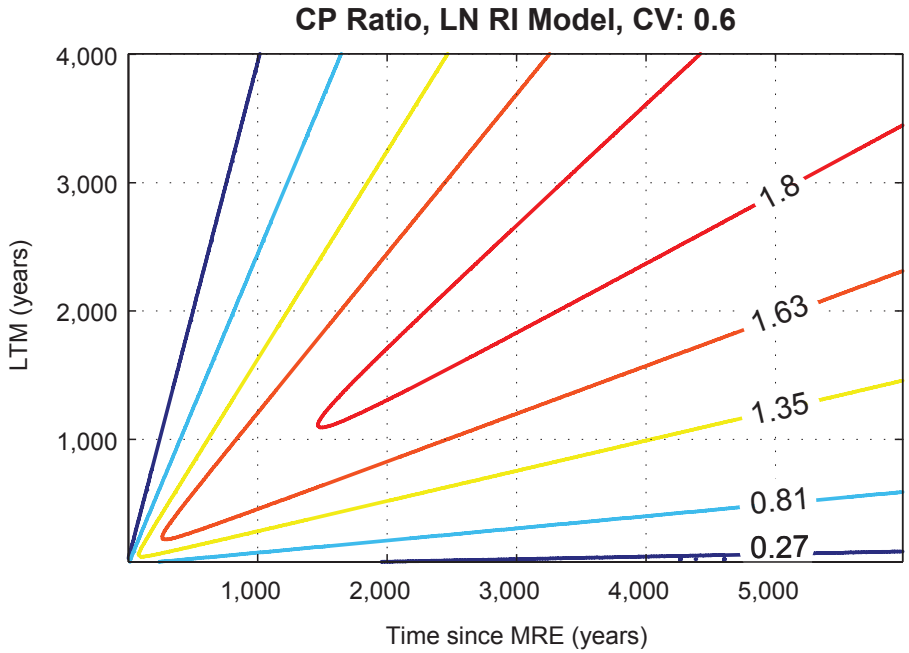

Note: Contours are the ratio of time-dependent rate to time-independent rate.
The long-term mean distribution is uniform on the range shown.

Conditional Probability Surface for the Lognormal Model, CV=0.6, and Slip Rate 1.7 mm/yr

DCPP SSC REPORT

Pacific Gas and Electric Company

Figure **H-6**

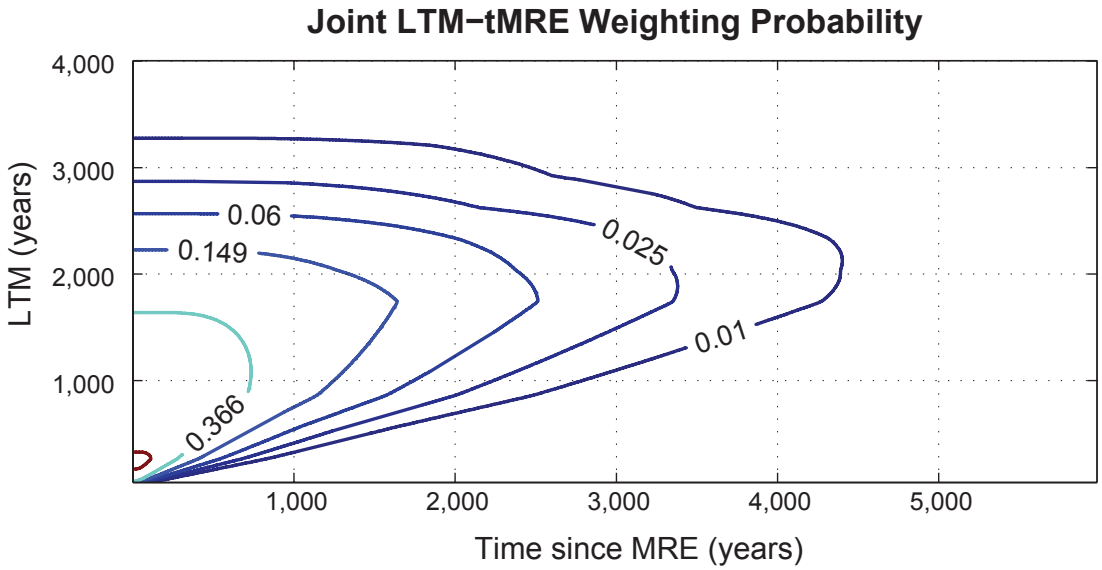

Notes:
- Slip rate = 1.7 mm/yr
- CV = 0.6
- T_{min} = 0. For other T_{min} values, weighting to left of T_{min} is not used.
- Hosgri fault displacement-per-event distribution is used.
- Joint probability has been divided by its maximum value to clarify relative weights of areas inside contours.

LTM-tMRE Joint Probability Surface Used to Select Regions in the Conditional Probability Ratio

DCPP SSC REPORT

Pacific Gas and Electric Company | Figure **H-7**

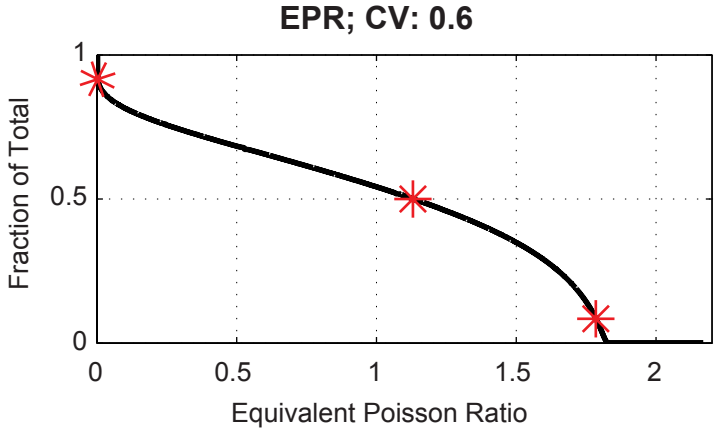

Note: Red stars mark the 91.5%, 50%, and 8.5% points used for three-point summaries by CV.
Fraction of total extends to 1.0.

Sorted Equivalent Poisson Ratio vs. Corresponding Cumulative Weight

DCPP SSC REPORT

Pacific Gas and Electric Company

Figure **H-8**

EPR, Lognormal Recurrence, CV=0.6, Four Historical T_{min} Cases

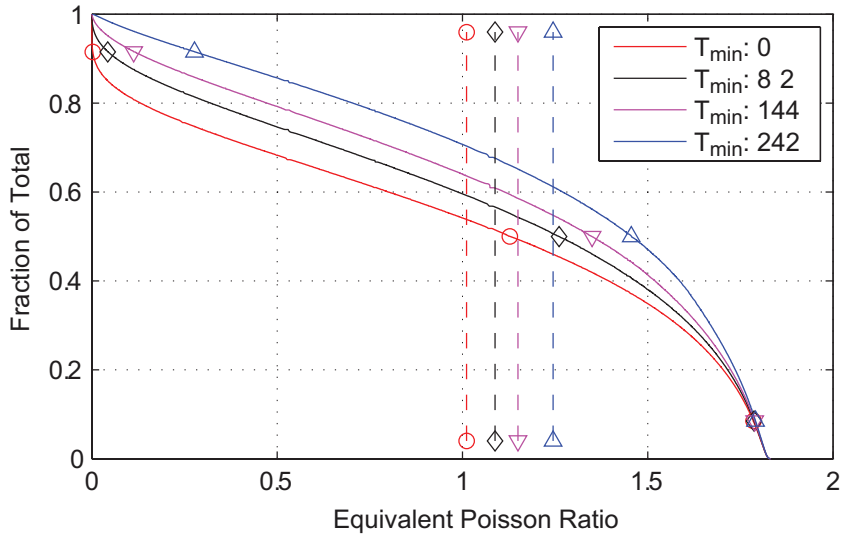

Note: Dashed lines are the weighted means corresponding by color and symbol to T_{min} cases.
Hosgri displacement-per-event profile is used for all curves.

Conditional Probability Ratios for Four Values of Historical Constraint T_{min}

DCPP SSC REPORT

Pacific Gas and Electric Company

Figure **H-9**

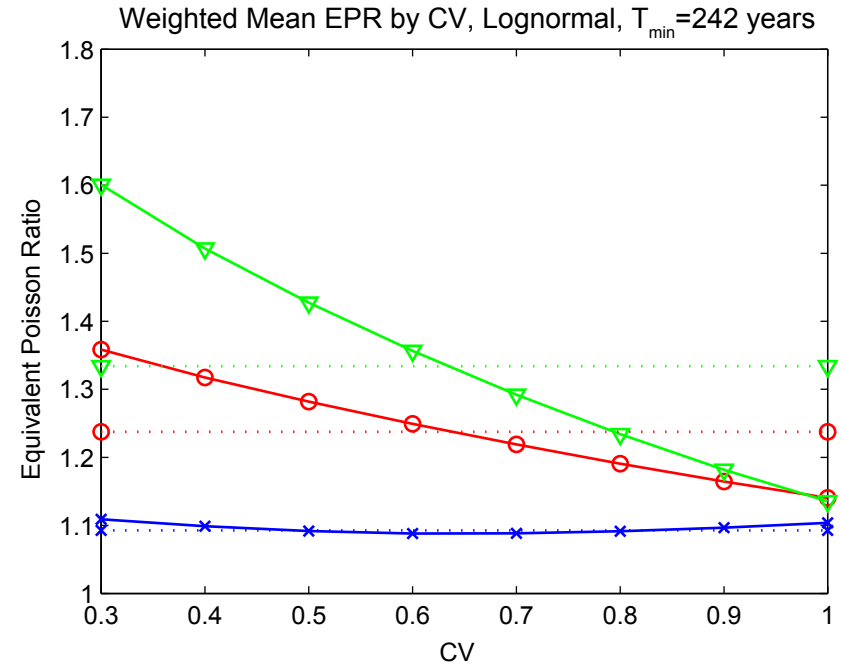

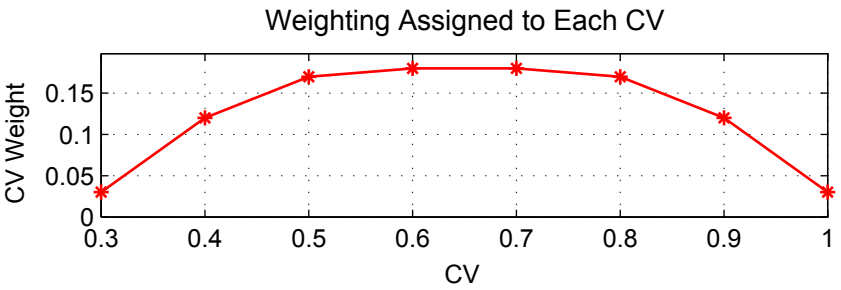

EXPLANATION

1.7 mm/yr

0.7 mm/yr

2.7 mm/yr

Notes:
- Dotted lines are CV-weighted mean values of corresponding solid lines.
- Hosgri displacement-per-event distribution is used for all cases.
- T_{min} is 242 years for all fault slip rates shown.

Weighted Mean Equivalent Poisson Ratio Estimates by Coefficient of Variation for the Lognormal Model and Three Fault Slip Rates

DCPP SSC REPORT

Pacific Gas and Electric Company

Figure **H-10**

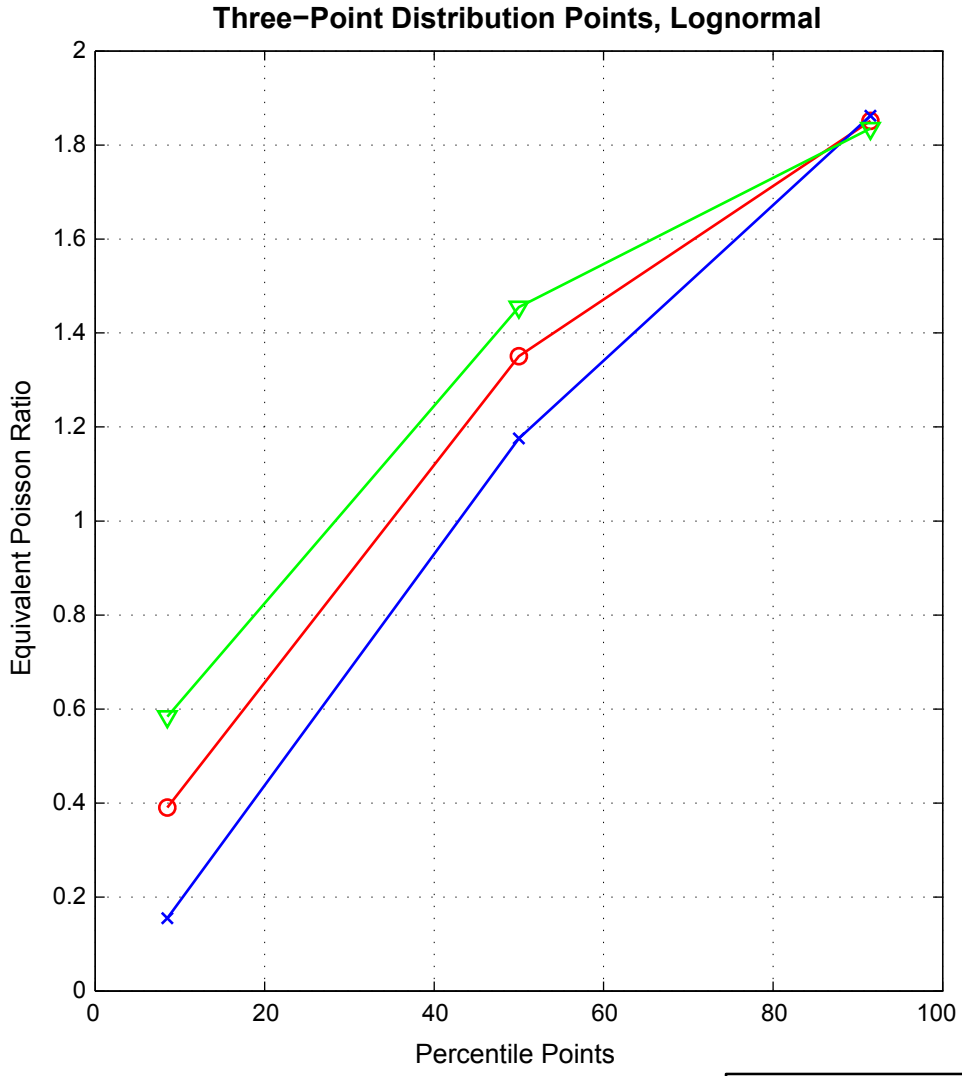

EXPLANATION

- 1.7 mm/yr
- 0.7 mm/yr
- 2.7 mm/yr

Note: T_{min} is 242 years for all fault slip rates shown.

Three-Point Distribution Equivalent Poisson Ratio Values for the Lognormal Model and Three Fault Slip Rates

DCPP SSC REPORT

Pacific Gas and Electric Company

Figure **H-11**

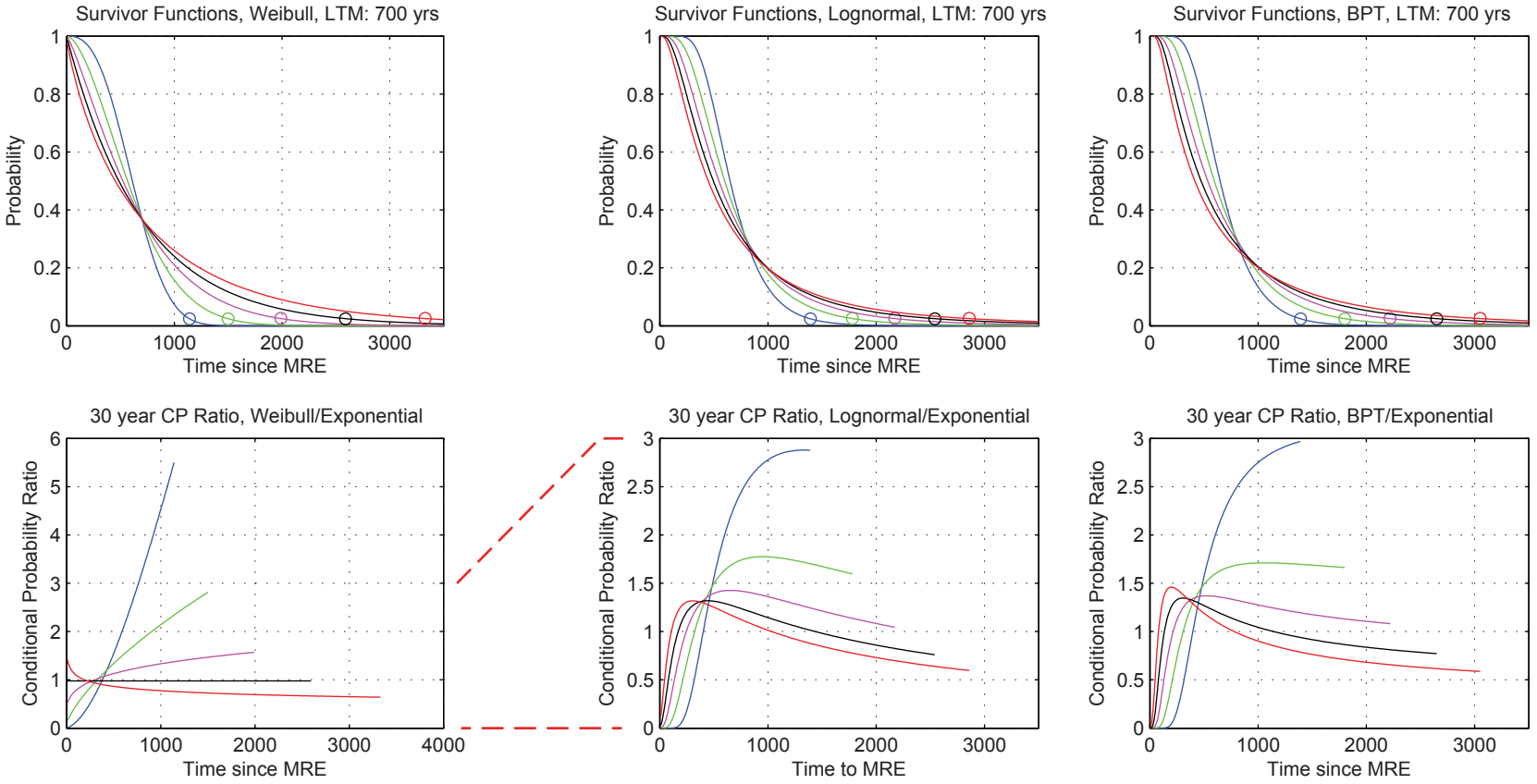

EXPLANATION

- CV = 0.4
- CV = 0.6
- CV = 0.8
- CV = 1.0
- CV = 1.2

Note: The long-term mean is 700 years for all cases shown.

Survivor Functions and Conditional Probability Ratios Compared for the Lognormal, BPT, and Weibull Distributions and Five Coefficient of Variation Values

DCPP SSC REPORT

Pacific Gas and Electric Company

Figure **H-12**

File path: S:\1005\005\Final_Report_Figures\Appendices_Figures\EPRI\Figure_H_12.ai; Date: 02/25/2015; User: Alex Remar, LCI; Rev.1

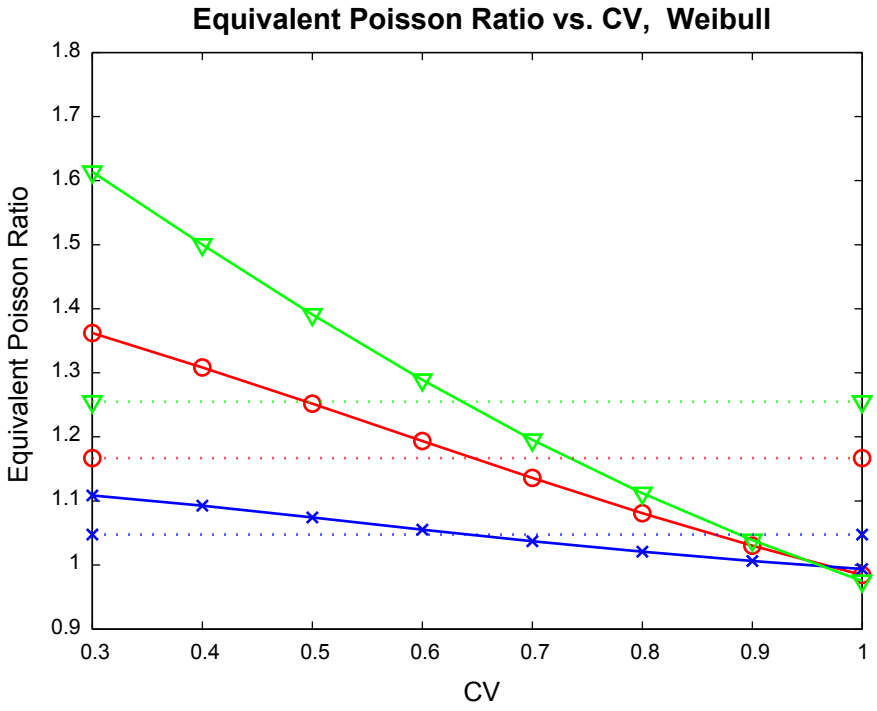

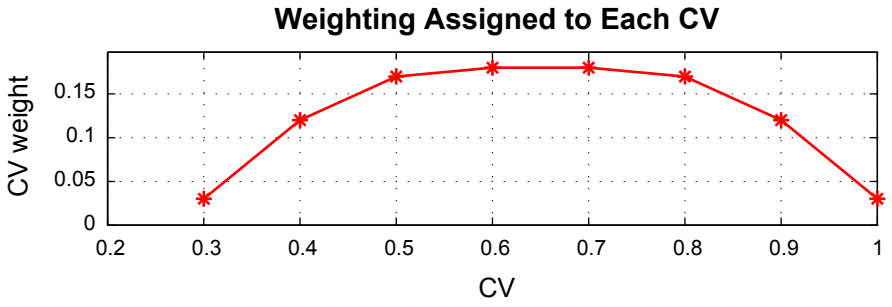

EXPLANATION

- 1.7 mm/yr
- 0.7 mm/yr
- 2.7 mm/yr

Notes:
- Dotted lines are CV-weighted mean values of corresponding solid lines.
- Hosgri displacement-per-event distribution is used for all cases.
- T_{min} is 242 years for all fault slip rates shown.

Per-Coefficient of Variation Equivalent Poisson Ratio Using the Weibull Recurrence Distribution for Three Fault Slip Rates

DCPP SSC REPORT

Pacific Gas and Electric Company

Figure **H-13**

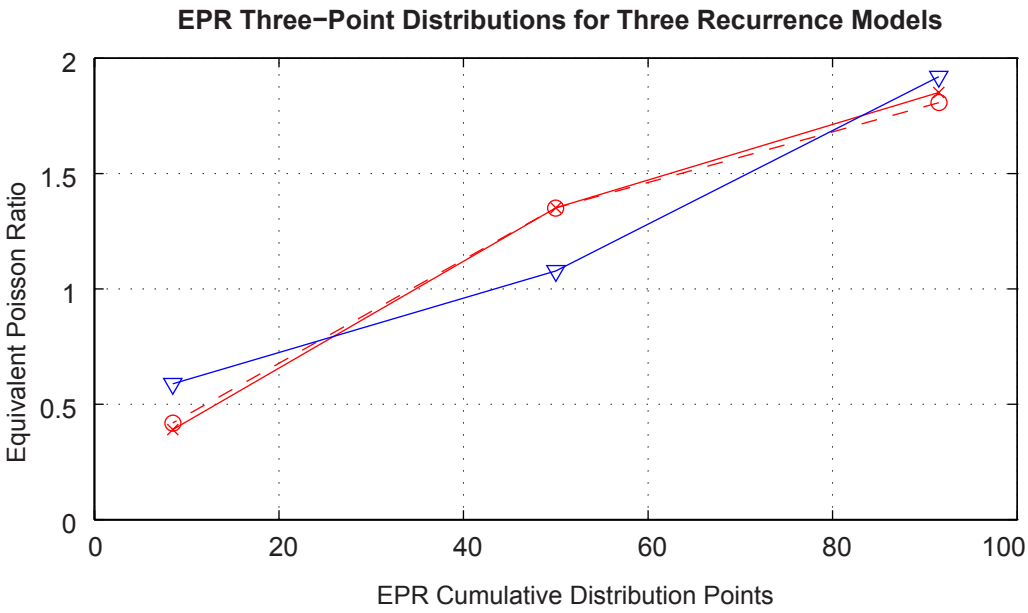

EXPLANATION

Lognormal

BPT

Weibull

Notes:
- Slip rate = 1.7 mm/yr for all recurrence models
- Lognormal points repeated from Figure H-11.
- CV weights as in Figure H-10 and H-13 are applied to per-CV EPR estimates at 8.5%, 50%, and 91.5% , and summed.

Coefficient of Variation Weighted Equivalent Poisson Ratio Distribution Points for Lognormal, BPT, and Weibull Recurrence Distributions

DCPP SSC REPORT

Pacific Gas and Electric Company

Figure **H-14**

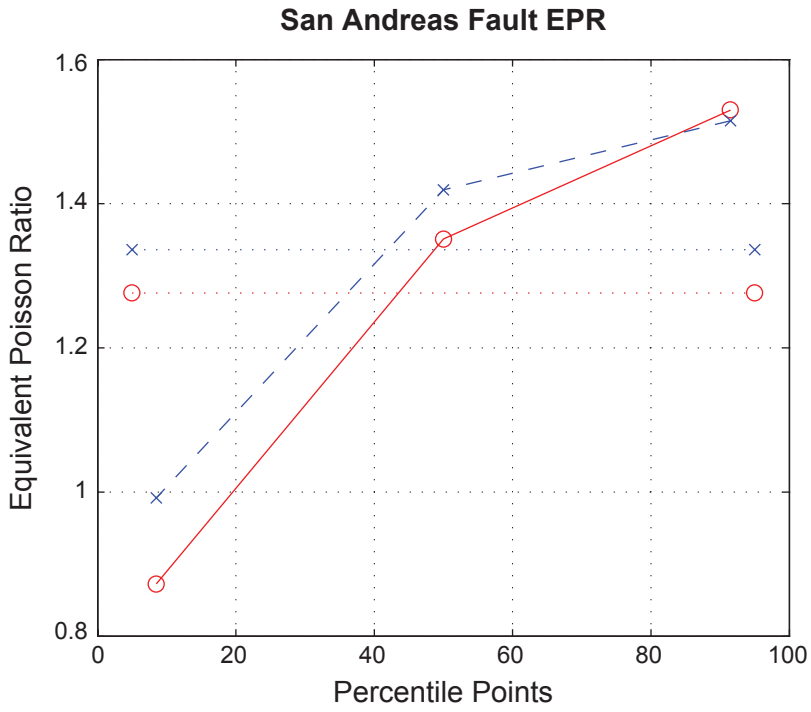

EXPLANATION

- tMRE ≥ 1857
- tMRE = 1857
- Weighted Mean ≥
- Weighted Mean =

San Andreas Fault Equivalent Poisson Ratio Estimation Comparing a Known MRE = 1857 to a Bounded MRE ≥ 1857

DCPP SSC REPORT

Pacific Gas and Electric Company

Figure **H-15**